Integrated modelling and multiscale gyrokinetic validation study of ETG turbulence in a JET hybrid H-mode scenario

J Citrin[1,2], S Maeyama[3], C Angioni[4], N Bonanomi[4], C Bourdelle[5], F.J Casson[6], E Fable[4], T Goerler[4], P Mantica[7], A Mariani[7], M Sertoli[4,6], G Staebler[8], T Watanabe[3] and JET contributors[*]

[1] DIFFER - Dutch Institute for Fundamental Energy Research, Eindhoven, the Netherlands
[2] Science and Technology of Nuclear Fusion Group, Eindhoven University of Technology, Eindhoven, Netherlands
[3] Department of Physics, Nagoya University, Nagoya 464-8602, Japan
[4] Max Planck Institute for Plasma Physics, Boltzmannstr. 2, 85748 Garching, Germany
[5] CEA, IRFM, F-13108 Saint Paul-lez-Durance, France
[6] CCFE, Culham Science Centre, Abingdon, OX14 3DB, United Kingdom of Great Britain and Northern Ireland
[7] Department of Physics "G. Occhialini", University of Milano-Bicocca, Institute for Plasma Science and Technology, CNR, Milano, Italy
[8] General Atomics, P.O. Box 85608 San Diego, California 92121, USA
[*] See the author list of 'Overview of JET results for optimising ITER operation' by J. Mailloux et al. to be published in Nuclear Fusion Special issue: Overview and Summary Papers from the 28th Fusion Energy Conference (Nice, France, 10-15 May 2021)

Abstract. Previous studies with first-principle-based integrated modelling suggested that ETG turbulence may lead to an anti-GyroBohm isotope scaling in JET high-performance hybrid H-mode scenarios. A dedicated comparison study against higher-fidelity turbulence modelling invalidates this claim. Ion-scale turbulence with magnetic field perturbations included, can match the power balance fluxes within temperature gradient error margins. Multiscale gyrokinetic simulations from two distinct codes produce no significant ETG heat flux, demonstrating that simple rules-of-thumb are insufficient criteria for its onset.

1 Introduction

An accurate predictive model for tokamak turbulent transport is a vital component of integrated tokamak simulation [1]. It enables physical interpretation of present-day experiments, scenario optimization, extrapolation to future scenarios and devices, and experimental design. The gyrokinetic framework has proven to be successful in quantitatively describing tokamak core turbulence [2], [3]. For sufficient tractability for application within integrated modelling suites, reduced-order-models applying the quasilinear approximation with saturation levels tuned to nonlinear gyrokinetic simulations have been developed, such as QuaLiKiz [4], [5] and TGLF [6]. While these models reproduce measured tokamak core thermodynamic radial profiles across wide regimes, continuous comparison against both experiments and higher fidelity simulation is necessary for validation of the models and their predictions for future scenarios and devices. This paper focuses on the validation of the QuaLiKiz model for predictions of Electron Temperature Gradient (ETG) driven turbulence in a specific JET scenario.

ETG turbulence is driven by modes on the electron Larmor-radius scale-length, where the ion response is essentially adiabatic due to finite Larmor radius effects. The relevant regimes in which ETG turbulence significantly contributes to electron heat transport is an open question. Gyrokinetic simulations on electron Larmor-radius scales have long showed the possibility that in spite of the small intrinsic ETG mode scale, extended radial streamers can provide experimentally relevant ETG mode driven electron heat fluxes [7], [8]. Experimentally, dedicated experiments have shown evidence of sharp electron temperature gradient thresholds consistent with ETG microturbulence [9], [10], and power-balance electron heat flux which cannot be reconciled in nonlinear gyrokinetic simulations by ion Larmor-radius scale (henceforth referred to as "ion-scale") fluxes [11]–[13]. In single-scale nonlinear ETG simulations with no ion-scale eddies, electron-scale zonal flows saturate ETG turbulence, leading to a collisionality scaling for the saturated ETG electron heat flux amplitude [14]. In nonlinear multiscale simulations with a realistic ion to electron mass ratio, a complex picture has emerged, involving cross-scale interactions [15]. ETG modes can weaken ion-scale zonal flows, increasing ion and electron transport on ion-scales. Ion-scale eddies can also suppress electron-scale streamers, quenching ETG electron heat transport in spite of linear ETG instability. Additional studies have shown that the cross-scale ETG quench depends on the strength of the ion-scale (ITG in the studies carried out) instability drive; for sufficiently low ion-scale drive, ETG streamers survive and can produce significant electron heat flux, explaining experimental observations in CMOD and DIII-D [16]–[18]. These simulations have led to proposed rules-of-thumb where significant ETG fluxes in multiscale simulations can be expected. In Ref. [19], the ratio $\gamma_{high-k}/\gamma_{low-k} \geq 40$ was correlated with significant cross-scale coupling. Refs. [20], [21] suggest the following as a necessary criteria for significant ETG fluxes:

$$\frac{\gamma}{k_y}|_{\text{high-k}} > \frac{\gamma}{k_y}|_{\text{low-k}} \tag{1}$$

where γ is the mode growth rate, k_y the binormal wavenumber, high-k corresponds to ETG scales $(0.1 < k_y\rho_e < 1)$ and low-k $(0.1 < k_y\rho_i < 1)$ corresponds to ion-scales, where $\rho_{e,i}$ is the electron/ion Larmor radius. For deuterium, $\rho_i/\rho_e \sim 60$, being the square root of the ion to electron mass ratio. At each scale the peak value of the ratios are taken. $MAX\left(\frac{\gamma}{k_y}|_{\text{low-k}}\right)$ is related to the zonal RMS $E \times B$ velocity under the hypothesis of a zonal flow k_x mixing saturation mechanism [22]. Additional hidden variables were not ruled out. The extreme computational expense of multiscale simulations, typically 10^7 CPUh for a single converged simulation, precludes extensive parameter variations for testing the rules' robustness.

A counter-example to a literal interpretation of the rule-of-thumb was recently shown in analysis of dedicated JET experiments [13]. In that work, high stiffness in the electron heat channel was experimentally observed, with insufficient electron heat flux predicted in ion-scale simulations. However, multiscale simulations with realistic input parameters did not produce significant ETG electron heat flux in spite of the linear calculations passing the threshold in Eq. 1.

Quasilinear turbulence models can incorporate such multiscale interactions into their saturation rules. QuaLiKiz has a simple rule, where ETG flux is quenched when the growth rate ratio between the peaks observed at electron -scales $0.1 < k_y\rho_e < 1$ and ion-scales $0.1 < k_y\rho_i < 1$, does not exceed the

square root of the ion to electron mass ratio [5]. TGLF employs a more refined zonal-flow mixing model to reproduce the phenomenology of multiscale nonlinear simulations [22]. The multiscale saturation rule was employed in a multi-hierarchy TGLF validation study against CMOD and AUG discharges pointing to ETG electron heat flux as a necessary component in half the cases [21]. The importance of ETG flux is also predicted for electron-heated DIII-D ITER baseline discharges [23].

This paper focuses on ETG predictions in the JET hybrid H-mode scenario (henceforth referred to as the 'hybrid scenario') which is one of two main operational scenarios being developed for the DT campaign. The hybrid scenario operates in a regime with improved confinement compared to the H_{98} scaling law at relatively reduced plasma current and density, with a tailored q-profile and increased MHD stability allowing operation at higher β_N [24]–[26]. Numerous mechanisms contribute to the improved confinement, including increased T_i/T_e, increased NBI source penetration, an optimized q-profile (broad inner $q \sim 1$ region with increased magnetic shear in the outer half-radius), increased $E \times B$ rotation shear, thermal and suprathermal-ion-enhanced electromagnetic (EM) stabilization of ITG, and increased Shafranov shift with virtuous core-edge coupling [27], [28].

The improved ion heat confinement and typical $T_i/T_e > 1$ in hybrid scenarios are expected to increase the potential importance of ETG turbulence; on the one hand through reduced ITG drive (see Eq. 1), and on the other hand through a decreased ETG critical gradient threshold, due to the $R/L_{Te}|_{\mathrm{crit}} \propto \left(1 + Z_{\mathrm{eff}} \frac{T_e}{T_i}\right)$ dependence [29]. In a recent multi-channel integrated modelling study devoted to heavy impurity prediction and control in the JET hybrid scenario [30], QuaLiKiz was applied for turbulent transport predictions within the JINTRAC [31], [32] integrated modelling suite. There, a significant role of ETG transport was predicted, with striking predictions in an isotope scan. The T_e profile was pinned to near the ETG critical threshold, regardless of main ion isotope. Then, with increasing isotope mass, the decreasing ion-electron heat exchange enabled T_i to increase, sustaining larger T_i/T_e and hence an increased ITG instability threshold, improving confinement and increasing T_i further, leading to an anti-GyroBohm ion mass confinement scaling. The larger T_i/T_e also decreases the ETG critical threshold, leading to a reduction of T_e, further increasing T_i/T_e and ITG stability. Without ETG, those feedback loops are not present and T_i/T_e is predicted closer to 1, with higher T_e and lower T_i. The mass scaling of the ion-electron heat exchange does not significantly impact the predicted confinement in the non-ETG case. We

Table 1: Basic parameters of JET hybrid discharge #94875 (pure deuterium), within the flattop time window analyzed. B_T is the vacuum toroidal magnetic field at the magnetic axis. I_p is the plasma current. P_{NBI} and P_{ICRH} are the Neutral Beam Injection (NBI) and Ion Cyclotron Resonance Heating (ICRH) total powers, respectively. $\beta_N \equiv \langle \beta \rangle \frac{aB_T}{I_p}$, where a is the minor radius.

B_T [T]	I_p [MA]	$P_{\mathrm{NBI}}[MW]$	$P_{\mathrm{ICRH}}[MW]$	β_N
2.8	2.2	27	6.1	2.3

note that the simulations scanning isotope mass both with and without ETG maintained the same pedestal parameters, fast ion distributions, and rotation, which may all impact isotope mass confinement scaling in general. Furthermore, the predicted anti-GyroBohm isotope scaling owing to parallel electron dynamics [33] is expected to play less of a role in ITG dominated H-modes, and in any case is not captured by QuaLiKiz.

The potential benefit of ETG turbulence for DT scenario extrapolations strongly motivates deeper validation of these predictions. This is the focus of the present paper. Since the JET discharge in Ref.[30] did not have core T_i measurements, a more recent hybrid scenario was selected for analysis. The rest of the paper is as follows: section 2 describes the JET discharge chosen for analysis and integrated modelling data preparation; section 3 describes the JINTRAC-QuaLiKiz integrated modelling of this discharge, and sensitivity studies to physics assumptions and QuaLiKiz version; section 4 describes the linear and nonlinear single-scale and multiscale gyrokinetic modelling of the discharge at a single radial point of interest, serving as a validation of QuaLiKiz predictions and a test of its assumptions; conclusions are provided in section 6. While this work focuses on ETG predictions and validation, including the ramifications of ETG for isotope confinement scaling, a related work has recently been published which studies - using integrated modelling - the isotope scaling predictions of this discharge more generally [34].

2 Characteristics of analyzed discharge and data preparation

We analyzed hybrid discharge #94875 from the JET C38 deuterium campaign. Its basic parameters are listed in Table 1. B_T, I_p, and total input power are the same as in hybrid discharge #92398 in Ref. [30], whose modelled ETG predictions have motivated the validation exercise in this paper. β_N is $\sim 10\%$ lower in discharge #94875. As opposed to #92398, discharge #94875 has high quality core T_i measurements, provided by Neon Charge Exchange (Ne CX) obtained through (trace) Ne seeding.

A time window of $t = 8.25 - 8.55$ s was chosen for analysis, at the beginning of the stationary-state
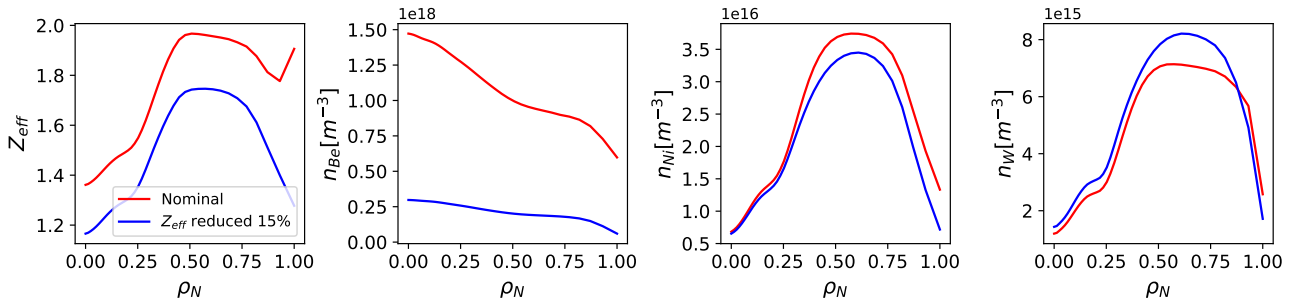
Figure 1: Flux-surface-averaged Z_{eff} and impurity densities as inferred from the method described in Ref. [35]. Both the nominal (red) and reduced within error bars (blue) Z_{eff} profiles are shown. The radiation inputs in the inference are the same in both cases.

flattop following the density buildup after the L-H transition. All kinetic profiles, source and equilibrium data, were averaged within this window. T_i and plasma rotation v_{tor} were measured with core and edge CX. T_e and n_e were measured with High Resolution Thomson Scattering (HRTS). Equilibrium reconstruction was carried out with EFIT++ [36]–[38] with kinetic constraints. The initial q-profile applied within integrated modelling was calculated by EFIT++. The kinetic profile fits – providing both initial condition and pedestal-top boundary conditions for the core integrated modelling – were carried out with Gaussian Process Regression using EX2GK [39], providing both fits and uncertainty envelopes. The NBI and ICRH (3.5% H-minority) deposition profiles were calculated by a TRANSP [40] interpretative simulation using NUBEAM [41] and TORIC [42]. The impurity profiles for Be, Ni, and W, were inferred by a method incorporating multiple diagnostics for constrained consistency [35]. Due to the significance of Z_{eff} in setting ETG stability [29], two sets of impurity profiles were generated, both nominal and propagating a 15% reduction on line-averaged Z_{eff} (lower bound of error bar). The measured radiation characteristics (with total $P_{\text{rad}} = 9.2MW$) were kept constant through simultaneous modification of Ni and W. The two sets of inferred impurity profiles are shown in figure 1. Sensitivity of ETG to Z_{eff} within integrated modelling is discussed in the next section.

3 Results from integrated modelling

The first step in the validation exercise is to ascertain whether QuaLiKiz can reproduce the kinetic profiles of the deuterium discharge #94875, and to investigate the predicted relevance of ETG turbulence. The QuaLiKiz quasilinear gyrokinetic turbulent transport model [4], [5], [43] is electrostatic, and limited to $\hat{s} - \alpha$ shifted circle geometry. Electromagnetic (EM) stabilization of ITG turbulence is taken into account through an ad-hoc model developed in Ref. [30], whereby the QuaLiKiz R/L_{Ti} input is locally reduced by the ratio of thermal to total (including suprathermal) pressure, $\frac{P_{\text{th}}}{P_{\text{supra}}+P_{\text{th}}}$. This approximates the impact of both thermal and suprathermal contributions to β stabilization of ITG.

Two versions of QuaLiKiz will be compared, QuaLiKiz 2.6.1 and QuaLiKiz 2.8.2. QuaLiKiz 2.6.1 is the version applied in Ref. [30], applied here to determine whether the same trends are observed in modelling of discharge #94875. These simulations are then compared to the most recent release 2.8.2 which includes two significant physics modifications compared to 2.6.1. Firstly, the Krook-like collision operator (ion-electron collisions for trapped electrons) was improved through comparison with higher-fidelity GENE [44] linear gyrokinetic simulations [45]. This improves the Trapped Electron Mode (TEM) dependence on collisionality, providing better density peaking predictions at mid to high values of collisionality, as well as increasing Q_e predicted on ion-scales in general. Secondly, the ETG saturation rule was recalibrated by reducing the ETG saturation level by factor 1/3 compared to Ref. [5] following comparison with ETG multiscale GENE simulations from Ref. [11]. In addition, the multiscale prefactor to the ETG saturation level was modified to be directly based on the $(\gamma/k)_{\text{max}}$ at each spectral scale. The version 2.6.1 multiscale prefactor was:

$$C_{\text{multiscale}} = \frac{1}{1 + e^{-\frac{1}{5}\left(\frac{\gamma_{\text{maxETG}}}{\gamma_{\text{maxITG}}} - \sqrt{\frac{m_i}{m_e}}\right)}} \quad (2)$$

and in 2.8.2 has been modified to:

$$C_{\text{multiscale}} = \frac{1}{1 + e^{-5\left(\frac{(\gamma/k)_{\text{maxETG}}}{(\gamma/k)_{\text{maxITG}}} - 1\right)}} \quad (3)$$

where the functional form is constructed such that this prefactor to the ETG flux approaches zero for $(\gamma/k)_{\text{maxITG}} > (\gamma/k)_{\text{maxETG}}$, and approaches unity for $(\gamma/k)_{\text{maxETG}} > (\gamma/k)_{\text{maxITG}}$, with a narrow transition zone between the two states. The linear eigenmodes on ρ_e scales are unchanged. The modification only impacts the saturation level.

Table 2: Description of predicted and prescribed physical quantities in the integrated modelling simulations

$n_{e,i}$	T_e	T_i	v_{tor}	n_{imp}	P_{rad}	j	Equilibrium
Predictive (for $\rho < 0.85$)	Predictive (for $\rho < 0.85$)	Predictive (for $\rho < 0.85$)	Prescribed	Prescribed (reconstruction)	Prescribed (bolometry)	Predictive	Prescribed (EFIT++)

Table 2 summarizes the list of predicted and prescribed physical quantities in the integrated modelling simulations discussed in the subsequent sections.

3.1 Integrated modelling with QuaLiKiz 2.6.1

QuaLiKiz 2.6.1 was run in JINTRAC for predictive simulations of discharge #94875. The measured T_e, T_i, n_e, v_{tor}, inferred q-profile, and inferred impurity content, were all set as initial conditions, corresponding to the averaged profiles in the $t = 8.25 - 8.55$ time-window. v_{tor} and impurities were left fixed. Heat and particle transport (deuterium and electrons), as well as current diffusion, were predictive. The simulation was run for 1 plasma second (several confinement times), sufficient for the temperature and density profiles to reach stationary state. The magnetic equilibrium was kept fixed at the pressure constrained EFIT++ solution. The NBI+RF heat and NBI particle sources were prescribed from the TRANSP solutions. The radiation sink was prescribed from bolometry. The core boundary condition was taken at normalized toroidal flux coordinate $\rho_N = 0.85$, just inside the pedestal top. The profiles were evolved only inside this boundary condition. Gas puff fuelling was neglected, since the penetration for $\rho_N < 0.85$ is negligible. The role of gas puff is captured by the prescribed density pedestal top. Neoclassical transport was calculated by NCLASS [46]. For the inner core, $\rho_N < 0.2$, a patch for electron heat transport was prescribed, as $\chi_e = e^{(-\rho/0.15)^2} \ [m/s^2]$. An exponential form was chosen to avoid any transport coefficient discontinuity, which may arise from a simple constant χ_e patch applied a limited radial range. The ad-hoc patch compensates for deep core anomalous transport not calculated by QuaLiKiz, needed to avoid spurious T_e peaking in the on-axis region. The missing transport cannot be explained by neoclassical transport which is negligible for the electron heat channel, nor by sawteeth which are absent or infrequent in hybrid scenarios. Recent work has indicated that KBM modes with elongated mode structures may be responsible for transport in this localized region [47]. These modes are challenging for QuaLiKiz to calculate due to both its electromagnetic and strongly ballooning eigenmode assumptions. In addition, non-local effects such as turbulence spreading could provide transport fluxes in this narrow region. Presently, QuaLiKiz does not incorporate any non-local effects.

The integrated modelling results are shown in figure 2, for the nominal Z_{eff} case. The predicted T_e, T_i and n_e profiles for $\rho_N < 0.85$ are all within 1σ of the fitted profile uncertainty envelopes, constituting a successful reproduction of the scenario.

The impact of Z_{eff} and ETG are shown in figure 3. Since density predictions are similar for all cases, only T_e and T_i are shown for brevity. Without the inclusion of ETG turbulence, the predicted T_e rises to levels above the GPR fit error envelope. Ion-scale turbulence alone - predicted by QuaLiKiz 2.6.1 to be ITG with a heat flux ratio of $Q_i/Qe \approx 4$ in this case - cannot sustain the nominal base-case $Q_i/Q_e \approx 2$ power balance ratio, which set by a combination of NBI power deposition (in this case ion dominated), ion-electron heat exchange (dependent on the $T_i - T_e$ temperature difference), and radiation. Therefore T_e must rise to decrease the ion-electron heat coupling, and increase Q_i/Q_e. The clear impact of Z_{eff} on the importance of predicted ETG turbulence is observable through the increased T_e difference between the with-ETG and no-ETG cases with 15% reduced Z_{eff}. Interestingly, T_i is *higher* for the cases with ETG, reminiscent of the anti-GyroBohm scaling of ion heat confinement in Ref. [30], where ETG clamps T_e and leads to increased T_i/T_e, improving ITG stability. The reduced Z_{eff} is within error bars. Its inclusion leads to predicted T_e still within the 1σ GPR uncertainty envelope. We therefore take the reduced Z_{eff} simulation with ETG as the "base-case" for subsequent sensitivity studies, and its output used for validation against higher-fidelity gyrokinetic models as reported in section 4.

The improved ion heat confinement regime typical of the hybrid scenario is predicted to rely on both $E \times B$ rotation shear and EM-stabilization, leading to higher T_i/T_e and further improving ion heat confinement. This is illustrated in figure 4. The base-case simulation is compared to a simulation where the QuaLiKiz $E \times B$ shear turbulence suppression model (see Refs. [5], [48]) is turned off, and to a simulation where additionally the ad-hoc EM-stabilization model is turned off. $E \times B$ shear is important in this scenario in the outer half radius, owing to the QuaLiKiz assumption of ignoring $E \times B$ in the inner half radius due to the underprediction of destabilizing parallel velocity gradient modes [5]. More dominant is the importance of the ad-hoc EM-stabilization rule, which increases on-axis T_i by $\sim 50\%$. While EM-stabilization has been shown to be critical for attaining high ion heat confinement in hybrid scenarios [28], including for this same discharge [34], we stress that the ad-hoc nature
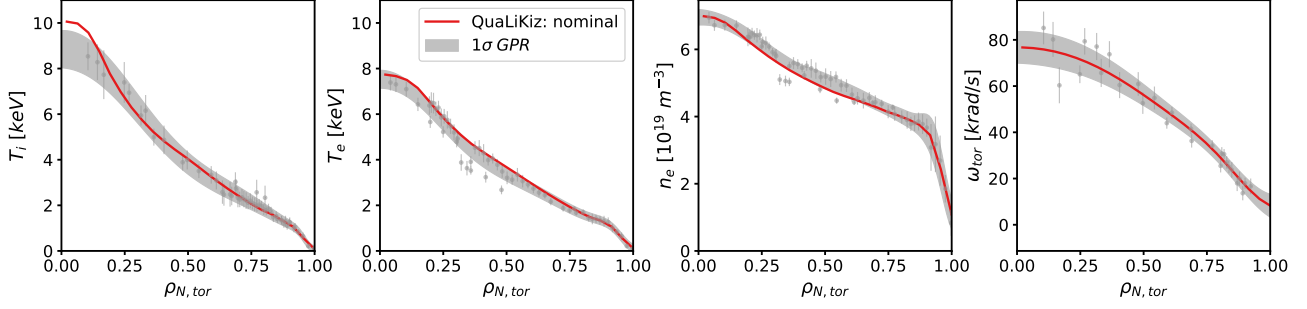
Figure 2: JINTRAC-QuaLiKiz_2.6.1 nominal Z_{eff} simulation of JET hybrid scenario discharge #94875. T_i, T_e, n_e predictions within the $\rho_N = 0.85$ boundary condition all agree with the Gaussian Process Regression (GPR) 1σ fit envelopes. The toroidal rotation (right panel) is prescribed
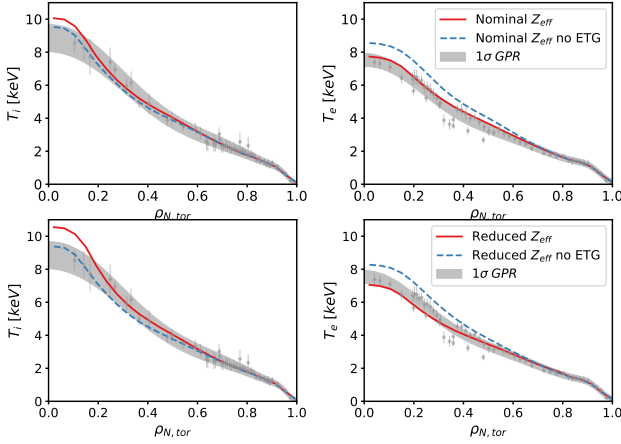

Figure 3: Comparison of JINTRAC-QuaLiKiz_2.6.1 predictions with nominal (upper plots) and reduced (lower plots) Z_{eff}, both with and without ETG. Only temperatures are shown for brevity

of the EM-stabilization rule in QuaLiKiz is a caveat, to be addressed in future work.

For the case without $E \times B$ and EM-stabilization, no ETG turbulence is predicted. This is a consequence of increased T_e/T_i and hence increased ETG critical thresholds, underlining the importance of improved ion confinement for attaining an ETG turbulence regime.

3.2 Integrated modelling with QuaLiKiz 2.8.2

Modelling #94875 with QuaLiKiz 2.6.1 indeed reproduces the same trends as in Ref. [30]. We now explore the differences obtained with the most recent QuaLiKiz release 2.8.2. Figure 5 shows the comparison for the deuterium (D) main ion base-case between QuaLiKiz 2.6.1 and 2.8.2. Predictions for T_e and T_i are similar. While 2.8.2 predicts slightly lowered temperatures (particularly for T_i), they are still predominantly within the 1σ error envelope. n_e is similar for both cases and omitted for brevity and clarity.

While predictions both versions agree with the measurements for the base-case, the new QuaLiKiz version has a significant modification of the impact of
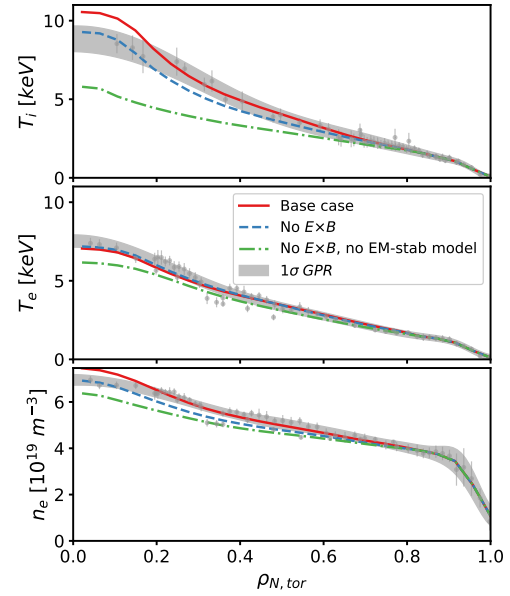

Figure 4: Comparison of JINTRAC-QuaLiKiz_2.6.1 predictions between the base-case, a case with the $E \times B$ rotation shear turbulence suppression model turned off, and a case with both $E \times B$ suppression and the EM-stabilization models turned off, for T_i (upper panel), T_e (middle panel), and n_e (lower panel) predictions

predicted electron-scale turbulence and hence on the isotope scaling. As shown in Figure 6, three separate simulations were carried out for each QuaLiKiz version: with D as main ion and ETG scales included (the base-case as in Figure 5), with D as main ion and ETG scales removed, and with tritium (T) as main ion and ETG scales included. A striking observation is that removing ETG turbulence from the QuaLiKiz 2.8.2 predictions has a reduced impact compared to the 2.6.1 predictions. This translates to a significantly reduced anti-GyroBohm isotope scaling in the T simulations. For 2.8.2, all three simulations in the physics scan provided very similar results. An explanation is that the increased trapped electron drive in 2.8.2 due to the improved collision operator has increased the electron heat flux component of the ion-scale modes, reducing

the necessity of electron-scale modes to supplement the electron heat flux. The fact that the improved collision operator in 2.8.2 is responsible for reduced impact of ETG in the integrated modelling, as opposed to the modified multiscale saturation rule in 2.8.2, was verified by running (not shown for brevity) a simulation using 2.8.2 with the 2.6.1 multiscale saturation rule, with similar results (both with and without ETG) to 2.8.2 itself. The impact of the improved collision operator on the linear modes is seen in figure 7, which shows a comparison of the QuaLiKiz linear growth rate and frequency predictions averaged over the last 100 ms of each respective base-case integrated modelling run, at $\rho = 0.65$. For version 2.6.1, the ion-scale modes ($k_\theta \rho_s < 2$) are purely ITG (positive frequencies - defined here as the ion diamagnetic direction). For version 2.8.2, TEM modes (negative frequencies in the electron diamagnetic direction) dominate the ion-scale spectra for $k_\theta \rho_s \geq 0.5$. These contribute to the electron heat flux. Also the ITG modes in 2.8.2 display an increased Q_e/Q_i compared to 2.6.1, further contributing to the ion-scale electron heat flux. In addition, in the 2.8.2 base-case simulation T_i/T_e is lower, increasing the power balance Q_i/Q_e ratio compared to the 2.6.1 case, easing the ability of ion-scale modes to provide the required flux, particularly when TEM plays a role. Figure 7 clearly shows that $(\gamma/k)_{\mathrm{ETG}} < (\gamma/k)_{\mathrm{ITG}}$ at $\rho = 0.65$ in the 2.8.2 simulation, while $(\gamma/k)_{\mathrm{ETG}} > (\gamma/k)_{\mathrm{ITG}}$ in 2.6.1, reflecting the relative importance of the role of ETG at the more outer radii in the simulations of the two different QuaLiKiz versions. At more inner radii ($\rho < 0.5$), ETG is unstable and relevant in both base-case simulations regardless of version.
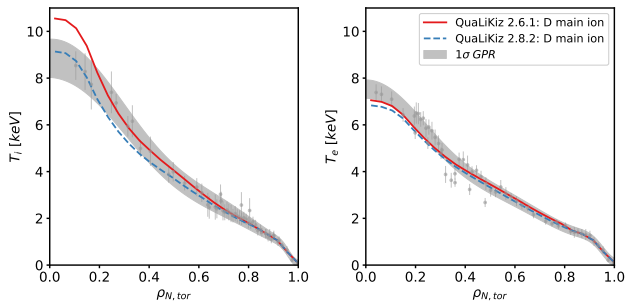
Figure 5: Comparison of JINTRAC-QuaLiKiz_2.6.1 and JINTRAC-QuaLiKiz_2.8.2 for the nominal Deuterium (D) main ion case. Predictions are shown for T_i (left column) and T_e (right column).

To summarize, JINTRAC-QuaLiKiz simulations of JET hybrid discharge #94875 using QuaLiKiz 2.6.1 agree with experimental measurements, and reproduce the phenomenology reported in Ref [30] regarding the importance of ETG turbulence and a mechanism for anti-GyroBohm isotope scaling. However, comparisons with the newer QuaLiKiz 2.8.2,

which has increased trapped electron drive owing to an improvement of the collision operator, leads to a decreased importance of ETG while still maintaining agreement with the experimental measurements within 1σ for the bulk of the profiles. With 2.8.2, the anti-GyroBohm isotope scaling predictions are significantly diminished. In the next section we proceed to a validation of QuaLiKiz predictions against higher-fidelity gyrokinetic modelling.
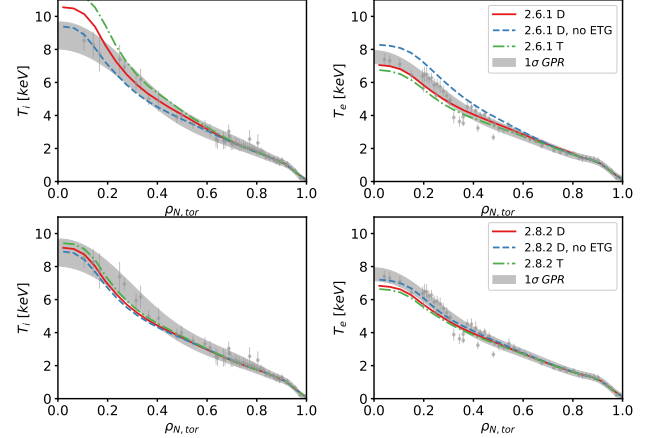
Figure 6: Comparison of JINTRAC-QuaLiKiz_2.6.1 and JINTRAC-QuaLiKiz_2.8.2 for ETG and isotope scaling predictions for discharge #94875. The upper row is QuaLiKiz 2.6.1, the lower row 2.8.2. Predictions are shown for T_i (left column) and T_e (right column).
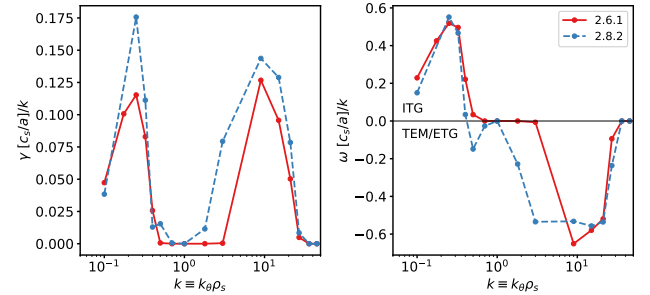
Figure 7: Comparison of JINTRAC-QuaLiKiz_2.6.1 and JINTRAC-QuaLiKiz_2.8.2 microstability predictions for the base-case integrated modelling run at $\rho = 0.65$. The ratio of growth rate γ to wavenumber k is shown in the left panel. γ is normalized by c_s/a, where $c_s \equiv \sqrt{T_e/m_i}$, and a is the minor radius. k is the poloidal wavenumber normalized by $1/\rho_s$, where the Larmor radius $\rho_s \equiv \sqrt{T_e m_i}/qB$. The ratio of mode frequency ω (same normalization as γ) to wavenumber k is shown in the right panel. The x-axis is logarithmic, to conveniently visualize both ion and electron scales.

4 Gyrokinetic analysis

In this section we validate QuaLiKiz 2.6.1 and 2.8.2 predictions against the higher-fidelity GENE gyrokinetic code, in its local, gradient-driven, δf mode. Both linear (with initial value solver) and

nonlinear GENE simulations were carried out. GENE is a Eulerian gyrokinetic code, evolving the perturbed particle distribution functions self-consistently with the Maxwell field equations. GENE works in field aligned coordinates, where x is the radial coordinate, z the parallel coordinate along the field line, and y the binormal coordinate. All shown simulations are spectral in both the x and y directions. Both $\hat{s} - \alpha$ (as in QuaLiKiz) and parameterized shaped Miller geometry [49] were employed, as detailed later in this section. Collisions in GENE were modelled using a linearised Landau-Boltzmann operator. Typical grid parameters were as follows: 24 point discretisation in the parallel direction, 48 points in the parallel velocity direction, and 15 magnetic moments, where parallel velocity box ranged between $[-3v_{Tj}, +3v_{Tj}]$, with thermal velocity $v_{Tj} = \sqrt{2T_j/m_j}$ where T_j is the background Maxwellian temperature, m the species mass, and j the species identifier. The upper end of the magnetic moment box was set at $9T_j/B_{\text{ref}}$, with B_{ref} the reference magnetic field strength (on-axis). For the linear runs, $n_{kx} = 31$ radial wavenumbers were included. For the ion-scale nonlinear runs, the perpendicular box sizes were $[L_x, L_y] \approx [100, 125]$ in units of ion Larmor radii, with $[n_{kx}, n_{ky}] = [128, 32]$ perpendicular wavenumbers included. The perpendicular grid parameters in the multiscale simulations are discussed in section 4.2. Numerical convergence was verified for all grid dimensions, both in the linear and nonlinear simulations, through a detailed study of the impact of modifying grid resolutions. All simulations carried out were electrostatic, unless explicitly specified in sensitivity tests.

All analysis was carried out for parameters corresponding to the final timeslice of the base-case integrated modelling simulation, at normalized toroidal flux coordinate $\rho = 0.65$. This is a location where ETG was predicted to significantly contribute to the electron heat flux according to the JINTRAC-QuaLiKiz_2.6.1 modelling. Moreover, this outward location is associated with lower-β, presumed to justify excluding electromagnetic (EM) ITG stabilization effects in the GENE modelling. The inclusion of EM effects in the nonlinear multiscale modelling would not be feasible due to the computational expense, particularly considering the long time-scale dynamics encountered when enhanced zonal flow coupling occurs [50]. At inner radii for this same discharge, EM effects are found to play a key role [34]. Modifications from the exact base-case parameters due to the desire to maintain power-balance relevant fluxes under the modelling assumptions (e.g. no rotation shear and EM effects) are mentioned where appropriate in the subsequent sections. See table 3

for a list of the main dimensionless input parameters, comparing the nominal measured values with the base-case JINTRAC-QuaLiKiz_2.6.1 predicted values used for the code comparison.

A further simplification of the modelling inputs was to bundle all impurity species into a single effective impurity. This single impurity was chosen with a charge, density, and density gradient, such that the main ion density and density gradient (n_D/n_e and R/L_{nD}) is unaltered compared to the 3-impurity case. Comparison of single-effective-impurity and 3-impurity GENE simulations (not shown for brevity) constituted a difference of under 5%, while saving significant computational time in the GENE simulations. The impact of fast ions on EM-stabilization of ITG is explored in dedicated linear simulations discussed in section 4.1.

4.1 Single scale simulations with simplified parameters

QuaLiKiz (both versions) and GENE (linear and nonlinear) simulations are compared in gradient-driven simulations: nonlinearly on ion scales only and linearly in both scales separately. The GENE simulations are carried out in $\hat{s} - \alpha$ geometry for a comparison with QuaLiKiz under similar geometry assumptions. Rotation is not included in the shown simulations, due to the induced non-stationary Floquet modes in GENE which hinders comparison.

An R/L_{Ti} scan comparing nonlinear GENE and quasilinear QuaLiKiz fluxes is shown in figure 8. The lack of rotation and EM-effects led to a power balance at an R/L_{Ti} value significantly below the measured one ($R/L_{Ti} \sim 8$). A number of observations are evident from the figure:

- GENE and QuaLiKiz agree on the base ITG stiffness level (sensitivity of ion heat flux to R/L_{Ti})

- QuaLiKiz ITG thresholds are upshifted compared to GENE by $R/L_{Ti} \approx 0.5$ for this case, a relatively minor difference of 10% in R/L_{Ti}

- At the R/L_{Ti} values corresponding to the ion heat flux power balance values (designated by the vertical lines), QuaLiKiz-2.8.2 and GENE agree on a heat flux ratio of $Q_i/Q_e \approx 2$. On the other hand, QuaLiKiz-2.6.1 has a significantly lower electron heat flux on ion-scales with $Q_i/Q_e \approx 4$. This underprediction of QuaLiKiz-2.6.1 ion-scale Q_e is consistent with other analysis of this same discharge at lower radii: see Fig.9b in Ref. [34].

- At R/L_{Ti} values below the power balance levels, QuaLiKiz-2.8.2 predicts a TEM dominated regime with $Q_e \gg Q_i$. This non-monotonic Q_e is in disagreement with GENE. This arises from an

Table 3: Dimensionless input parameters for the GENE vs QuaLiKiz single-scale study, including comparison of the nominal measured values to the values from the final timeslice of the base-case integrated modelling simulation used for the code comparison

Case	R/L_{Ti}	R/L_{Te}	R/L_{ne}	$\hat{s}$	q	T_i/T_e	α	Z_{eff}
JINTRAC-QuaLiKiz_2.6.1 (base-case)	9.25	8.62	2.93	1.5	2.02	1.08	0.62	1.65
Measured	8.03	8.72	3.46	1.4	2.1	1.12	0.71	1.55

over-prediction of TEM drive in QuaLiKiz in the low R/L_{Ti} regime at these parameters. We stress that for this case, the disagreement occurs in a Q_i range significantly below power-balance levels and thus does not impact the scenario prediction.

We can conclude - in the regime of physical interest at power balance levels - that QuaLiKiz-2.8.2 is better validated by the GENE comparison than QuaLiKiz-2.6.1. The increased electron heat flux is consistent with the increase in TEM drive due to the collision operator improvement, underpinning the reduced reliance in 2.8.2 on ETG to supplement the electron heat flux in the integrated modelling simulations.

Regarding the impact of rotation, not shown for brevity, additional nonlinear-GENE and QuaLiKiz R/L_{Ti} scans where carried out with $E \times B$ shear included. This had a similar impact for both models, leading to an R/L_{Ti} upshift of ≈ 1.
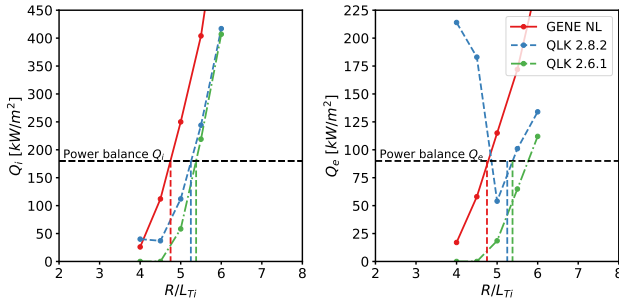

Figure 8: Comparison between JINTRAC-QuaLiKiz_2.6.1 (green dashed curves), JINTRAC-QuaLiKiz_2.8.2 (blue dashed curves), and nonlinear GENE (red solid curves) ion and electron heat flux predictions for the base-case integrated modelling run. The power balance heat fluxes from the integrated modelling run are portrayed by the horizontal black dashed lines. The red, blue, and green vertical dashed lines portray the R/L_{Ti} corresponding to the Q_i power balance levels for the GENE, QuaLiKiz 2.8.1, and QuaLiKiz 2.6.1 simulations respectively.

The trends observed in figure 8 can be understood from examination of the underlying linear modes. This is shown in figure 9. In the left panel, both QuaLiKiz-2.6.1 and 2.8.2 have reduced ITG growth rates compared to GENE. This growth-rate discrepancy is mostly resolved by a 15% increase in R/L_{Ti} (see right panel), consistent with the power-balance R/L_{Ti} shift in figure 8. QuaLiKiz-2.6.1 has no TEM (interpreted as electron modes on ion-scales), whereas QuaLiKiz-2.8.2 has TEM growth rates above GENE, consistent with the TEM-dominated regime

at low R/L_{Ti}. Finally, GENE ETG growth rates are significant, with maximum γ/k_{ETG} approximately twice maximum γ/k_{ITG}. This suggests that multiscale simulations should lead to significant ETG flux. This is not necessarily borne out, as will be discussed in section 4.2. The QuaLiKiz ETG growth rates are in line with GENE growth rates following a 15% R/L_{Te} increase. The fact that seemingly significant growth rate discrepancies are resolved by relatively minor modifications in driving gradient is typical of the challenges faced by gradient-driven comparisons.
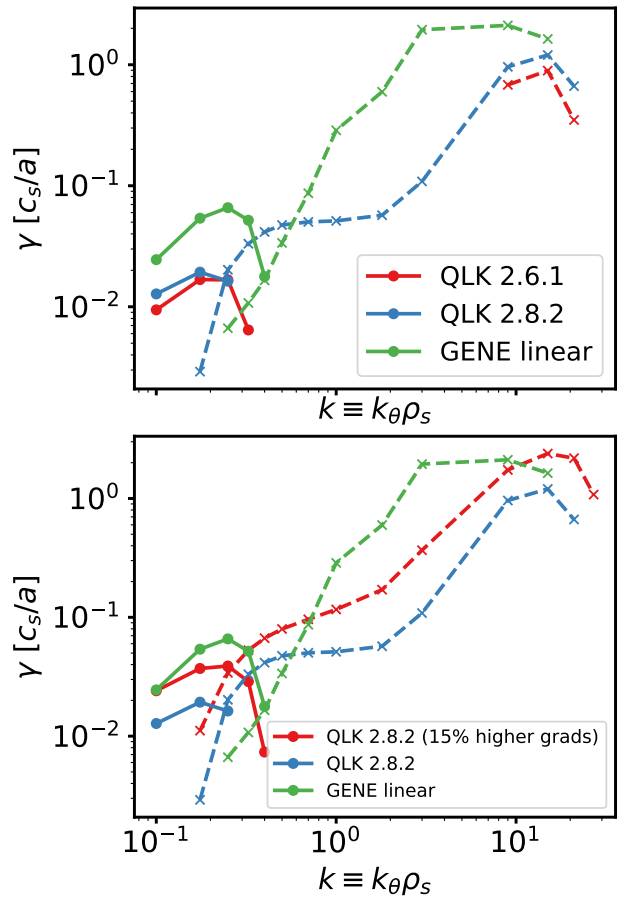

Figure 9: Comparison between QuaLiKiz and GENE linear spectra for the same parameters as in figure 8, at R/L_{Ti}=5.4. The upper panel compares QuaLiKiz-2.6.1 (red) QuaLiKiz-2.8.2 (blue), and linear GENE (green). Ion modes (ITG) are represented by the solid curves, and electron modes (TEM+ETG) by dashed curves. In the lower panel, QuaLiKiz-2.6.1 is absent and the red curves correspond to QuaLiKiz-2.8.2 for both R/L_{Ti} and R/L_{Te} increased by 15%

This section concludes with a study of the impact

Table 4: Fast ion (D-NBI) species parameters for the linear GENE EM simulations shown in figure 10. Parameters were calculated from the TRANSP-NUBEAM interpretative simulation results prescribed in the predictive integrated modelling

n_{fast}/n_e	T_{fast}/T_e [MA]	R/L_{Tfast}	R/L_{nfast}
0.0434	11.24	3.81	11.24

of EM-stabilization, to judge *a posteriori* whether EM effects can indeed be neglected at the relatively outward radius of $\rho = 0.65$ chosen for analysis of this case. Four cases were studied with linear GENE, with parameters as in figure 9 but increased ITG drive (R/L_{Ti}= 8.3), close to the experimentally measured value, such that the EM-stabilization impact on the nominal parameters is clearer. The electrostatic (ES) case ($\beta = 0$) is compared with the EM case with nominal $\beta = 0.68\%$, and with the addition of fast ions from the NBI heating, assuming Maxwellian fast ions with parameters taken from the TRANSP-NUBEAM modelling (see table 4). α_{MHD} is kept fixed at the nominal value throughout. The inclusion of EM effects provides a very significant stabilization, as evident from the drop in growth rates from the red to blue curves. At the lowest k, a mode of a microtearing type is then dominant, although this is not expected to lead to significant flux in nonlinear modelling in conjunction with ITG [51]. The growth rates are further reduced with the inclusion of fast ions across much of the spectrum. However, for nominal fast ions, a fast-ion driven mode dominates the spectrum at the lowest k. Nonlinearly, such modes in JET hybrid scenarios are predicted to drive significant thermal and fast-ion transport, and thus in a self-organized state are expected to remain marginally subcritical through self-consistent profile modifications [28], although flux-driven high-fidelity modelling is necessary to shed light on the precise system dynamics. A modest 20% reduction in fast-ion parameters (density and gradients) suppresses this mode, as seen in the purple curve.

This phenomenology is strongly reminiscent of the typical observations at more inner radii in hybrid scenarios, see e.g. Ref. [28]. While striking that it is observed here at outer radii, the observation is also strongly geometry dependent. As later analyzed in section 4.3, the linear EM-stabilization effect is weakened with shaped geometry.

4.2 Multiscale simulations with simplified parameters

The importance of EM-stabilization highlighted in the previous section, led to the realisation that it was not feasible (due to the computational expense of finite-β simulations, particularly when long time-scale
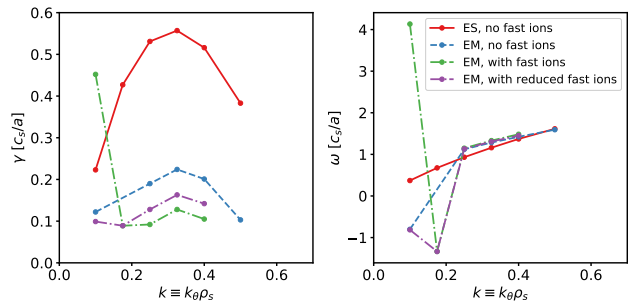

Figure 10: Study of the impact of EM-stabilization in GENE $\hat{s} - \alpha$ linear runs. Parameters are the same as in figure 9, but with $R/L_{Ti}=R/L_{Te}$=8.3. Ion-scale growth rate spectra are compared for: an electrostatic case (red), electromagnetic case with the true physical $\beta = 0.68\%$ (blue), with nominal fast ions included (green), and with reduced fast ions (purple) where fast ion density and gradients were reduced by 20%. Growth rates are shown in the left panel, frequencies in the right panel

dynamics are necessary for convergence) to carry out multiscale simulations with sufficient physical realism to correspond directly to the experimental setting. Instead, it was decided to proceed with a reduced physics setting with parameters close to, but not exactly corresponding, to the experimental parameters. See table 5 for a comparison. The physical D/e mass ratio was applied throughout. The main reduction in computational cost is due to using a single ion species ($Z_{eff} = 1$). R/L_{Ti}= 6.25 was set to match the ion heat flux in a single-scale nonlinear simulation to the experimental power balance value. R/L_{Te}= 8 was set to ensure strongly linearly unstable ETG such that the maximum γ/k_y on ETG scales was approximately factor 2 of the maximum γ/k_y on ITG scales. This ratio suggests that ETG should play a significant role in the subsequent multiscale simulation. The goal is then to validate QuaLiKiz ETG predictions in an expected clearly ETG-relevant case. R/L_{ne} was set to 2.3. Both QuaLiKiz-2.6.1 and 2.8.2 predict Q_e caused by high-k ETG fluctuations to approximately equal Q_i caused by low-k ITG fluctuations, leading to a $Q_e \approx Q_i$ scenario since ITG $Q_i/Q_e \approx 5$ for these parameters.

Both GENE and the GKV [52], [53] gyrokinetic codes were applied for the study, to increase validation robustness and to benchmark multiscale predictions between the two different codes. The numerical grid resolution settings are shown in table 6.

The linear benchmark between GKV and GENE for both ion and electron scales is shown in figure 11. The codes agree for both spatial-scales, with minor differences observed in ion-scales on the order of 20%. A like-for-like benchmark was not feasible here since the two codes applied different collision operators: GENE a linearized Landau-Bolzmann operator and GKV a Sugama collision operator. This may be the reason for the more extensive relative difference at $k_y = 0.4$ which was at the ITG-TEM boundary, and

Table 5: Main dimensionless physical input parameters applied for the GENE and GKV multiscale study, compared with the JINTRAC-QuaLiKiz_2.6.1 base-case values used in the single-scale study in section 3. ϵ is the local inverse aspect ratio. Dimensional reference parameters (e.g. for collisionality calculations) were $T_{ref} = 2.56 \; keV$, $n_{ref} = 4.87 \cdot 10^{19} \; m^{-3}$, $L_{ref} = 3.06 \; m$.

Case	R/L_{Ti}	R/L_{Te}	R/L_{ne}	$\hat{s}$	q	T_i/T_e	α	Z_{eff}	ϵ
Nominal	9.25	8.62	2.93	1.5	2.02	1.08	0.62	1.65	0.67
Multiscale study	6.25	8	2.3	1.5	2.02	1.08	0	1	0.67

Table 6: GENE and GKV grid resolution for the multiscale study. L_x is radial box size in reference ion Larmor units. n_{kx} is the number of radial modes. $k_{y(min)}$ is the minimum normalized wavenumber. n_z is the parallel resolution. n_v and n_w are parallel velocity and perpendicular velocity (magnetic moments) resolution respectively

Code	L_x	n_{kx}	$k_{y(min)}$	n_{ky}	n_z	n_v	n_w
GENE	47.5	500	0.1	620	32	48	16
GKV	49.5	340	0.08	339	32	48	24

hence extremely sensitive to the collision operator. However, the low growth rate at that k_y means that the impact on the fluxes is negligible.
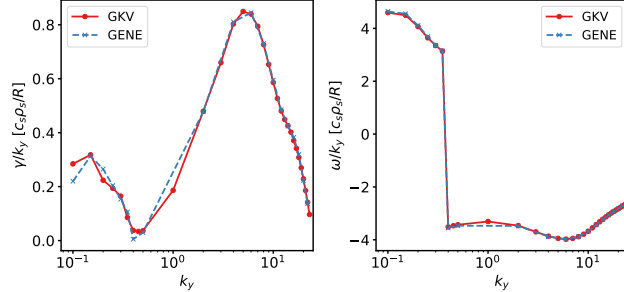
Figure 11: Linear benchmark between GKV and GENE for the multiscale parameters for growth rates (left panel) and frequencies (right panel). Both ion and electron scales are shown with a logarithmic x-axis. The growth rates and frequencies are normalized by the wavenumber k_y to maintain similar magnitudes on both ion and electron Larmor radius scales. Modes in the ion diamagnetic direction are defined as having positive frequencies.
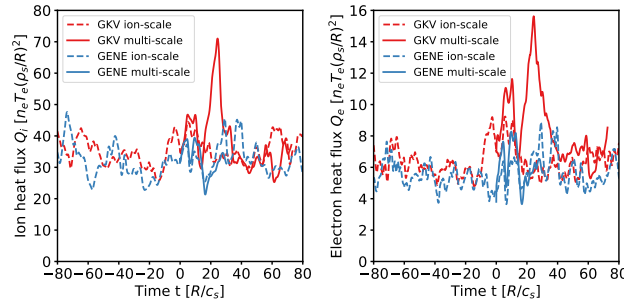
Figure 12: Temporal evolution of the electron (right panel) and ion (left panel) heat fluxes in GKV (red) and GENE (blue) ion-scale (dashed) and multiscale (solid) simulations based on the same physical inputs. The zero in the time axis corresponds to the time when the multiscale simulations are initialized based on the corresponding ion-scale simulation checkpoint. The multiscale GKV and GENE simulations do not show a significant addition to the electron heat flux compared to the ion-scale simulations
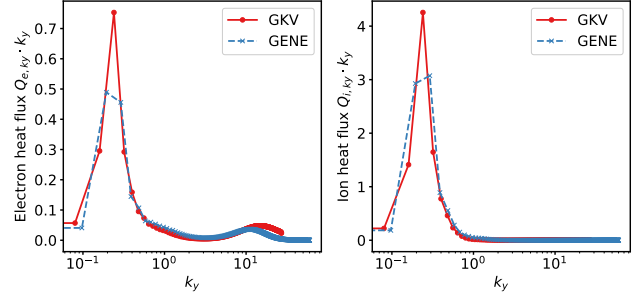
Figure 13: GENE and GKV ion (right panel) and electron (left panel) heat flux spectra in a logx plot. The y-axis is $Q_e \cdot k_y$, such that the areas under the curves in the logx plot correspond to the total heat flux. Less than 10% of the electron heat flux is from electron scales. The heat fluxes are in GyroBohm units with $T_{\text{ref}} = T_e$ and $L_{\text{ref}} = R_{\text{maj}}$.

In the following we discuss the results of the multiscale nonlinear simulations. The central and most striking result of this work, is that in spite of the linear $(\gamma/k_y)_{\text{maxETG}} \approx 2\,(\gamma/k_y)_{\text{maxITG}}$, the multiscale simulations did not produce significant ETG heat flux. The results are shown in figures 12 and 13. In figure 12, GKV and GENE ion-scale and multiscale simulations are compared. The multiscale simulations were initiated from a checkpoint at a quasi-stationary phase of the corresponding ion-scale nonlinear simulations, and continued for sufficient time to determine whether ETG flux emerges and saturates (see e.g. Fig.1 in Ref. [54]). This technique allows for faster general convergence by having a good initial condition for the ion-scale (k_x, k_y) in the multiscale simulation. Only an initial transient phase showed an increase in both ion and electron heat fluxes (more evident in the GKV simulations), with the fluxes then converging back to a similar level as the ion-scale simulation. No significant ETG fluxes are predicted. This is further seen in figure 13, where the heat flux spectra from the GKV and GENE multiscale simulations are compared. Both codes predict that only $< 10\%$ of the electron heat flux arises from electron-scales. A summary of the predicted fluxes by both GENE and GKV multiscale simulations is provided in table 7.

These results are a counter-example to the classification suggested in Ref. [21] (see figure 2 therein). Our case has weak linear TEM and strong linear ETG modes in comparison to the ITG modes, which according to Ref. [21] are criteria which should correlate with the importance of multiscale effects.

Table 7: Summary of nonlinear multiscale GENE and GKV ion and electron heat fluxes, averaged over the final 20 time units (in $[R/c_s]$) in their respective simulations. The mean and standard deviation of the fluxes in that time window are provided.

Code	Q_i	Q_e
GENE	30.5±4.5	5.9±1.2
GKV	32.6±3.9	6.8±0.8

However, we found only weak multiscale effects, hinting at the importance of additional parameters. The results also demonstrate that the rule-of-thumb suggested in Ref. [19] is an insufficient criteria for the onset of significant ETG fluxes. However, generality of this rule was not claimed and due to the relatively small number of multiscale simulations studied, Ref. [19] does not exclude dependence on additional quantities. Furthermore, the related Eq 1 is stated in Ref. [20] as being the non-linear threshold for when ETG linearly exceeds the total suppression due to zonal flow mixing. This does seem to be satisfied in our case, due to the finite (but low) electron-scale bump in the electron heat flux spectrum in figure 13. However, exceeding the non-linear threshold for ETG turbulence does not necessarily correlate to significant ETG flux, which also requires the existence of significant ETG streamers – elongated structures with $k_x \ll k_y$ on electron Larmor radius scales – which are absent in this case. The k_x spectrum is geometry dependent [55]. Unfortunately there was insufficient computational resources to rerun our cases with more realistic geometry to investigate its impact on ETG streamers.

We note that while R/L_{Ti} was set to match the power-balance heat flux in the ion-scale simulations, multiscale effects can in principle degrade ion-scale zonal flows and enhance ion-scale flux [15]. There were insufficient HPC resources to carry out further multiscale simulations at decreased R/L_{Ti} to examine whether in that case significant ETG flux would emerge, with multiscale effects then raising Q_i up to power-balance consistent values.

To summarize: the multiscale runs carried out showed a lack of significant ETG flux in spite of the strong relative electron to ion scale linear drive. Further investigation of the dependencies which lead to the emergence of significant ETG flux, in cases where the nonlinear ETG threshold has been passed, is out of the scope of this paper. Clearly, there are hidden variables at play which complicate the existence criteria of significant ETG flux beyond simple rules-of-thumb based on the γ/k ratios. QuaLiKiz ETG predictions are not validated for this specific parameter set. A more extensive study is necessary to calibrate the QuaLiKiz multiscale rule and quasilinear transport model multiscale saturation rules in general. We note that the cases studied in Refs. [19], [21], where the rule-of-thumb applies, are in the $Q_e > Q_i$ regime

where TEM modes fill the spectral gap between ion and electron scales (see also Figure 5 in Ref. [20], whereas the cases studied here are in the $Q_i > Q_e$ regime with no spectral gap, as evident in Figure 11. The ramifications of heat flux ratios on the turbulence regime, spectral gap, and subsequent multiscale impact is left for future work, as is the magnetic geometry impact on streamer formation.

4.3 Ion-scale simulations with full physics

The multiscale results from the previous section suggest that ETG turbulence is not important at $\rho = 0.65$ for the discharge studied. This leads to the question of whether ion-scale turbulence in high-fidelity simulations like GENE or GKV is sufficient to describe the experimental power balance at the measured kinetic profile gradients for both ion and electron heat flux. We tackle this question when including full-physics on ion-scales, with Miller parameterized geometry [49], inclusion of $E \times B$ shear, EM-effects, and fast ions. Due to limitations of computational time, we limit this study to $\rho = 0.65$, and apply GENE only. A single effective impurity species was used to save computational cost, maintaining the same impact on main ion dilution and R/L_{ni} as the full set of impurities.

Nonlinear simulations using the nominal measured input parameters (see table 3, led to predicted heat fluxes of $Q_i \approx 490 \ kW/m^2$ and $Q_e \approx 240 \ kW/m^2$, significantly above the power balance heat fluxes of $Q_i \approx 180 \ kW/m^2$ and $Q_e \approx 90 \ kW/m^2$. Therefore, an R/L_{Ti} scan was carried out with both R/L_{Te} and R/L_{ne} reduced by 20%, within their error bars. The results are shown in figure 14. The main finding is that experimental power balance is predicted, with the correct experimental heat flux ratio of $Q_i/Q_e \approx 2$, within 5% of the measured R/L_{Ti} when both R/L_{Te} and R/L_{ne} are reduced by 20%. While not the focus of the paper and not shown for brevity, particle transport was overpredicted by a factor ~ 2 and momentum transport underpredicted by a factor ~ 2. More extensive uncertainty quantification including propagation of gradient, magnetic equilibrium, fast ion, and impurity uncertainties, and an attempt to simultaneously match all transport channels within these input certainties, was not feasible due to lack of resources. However, the limited uncertainty quantification performed already demonstrates that ion-scale turbulence predictions provides a consistent description of the heat fluxes, and that it is not necessary to invoke ETG turbulence to describe the electron heat flux for this case.

In the course of this exercise, a number of interesting observations were made regarding the impact of EM-effects at finite-β. These are described
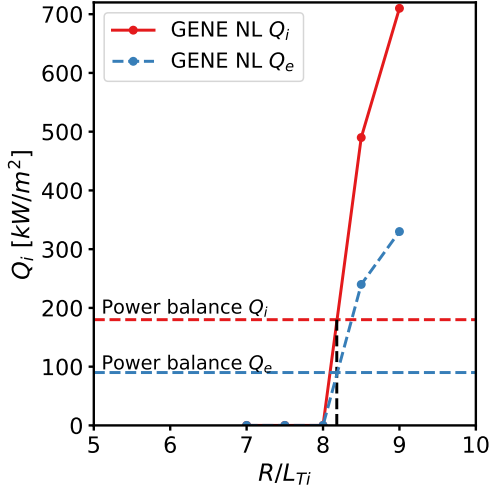
Figure 14: Nonlinear GENE ion heat flux (red) and electron heat flux (blue) predictions in a R/L_{Ti} scan at $\rho = 0.65$ with both R/L_{Te} and R/L_{ne} are reduced by 20%. The power balance heat fluxes from the integrated modelling run are portrayed by the horizontal dashed lines. Measured $R/L_{Ti} \approx 8$
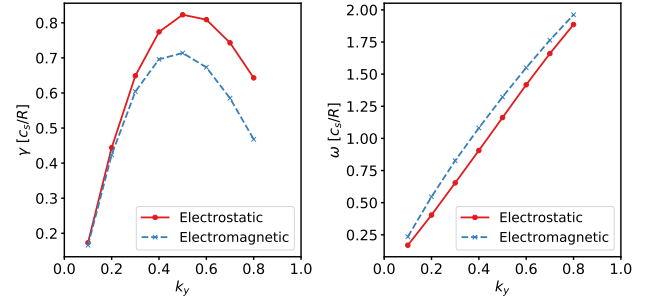

Figure 15: Electrostatic (red curves) vs electromagnetic (blue curves) linear GENE simulations with Miller geometry, at nominal R/L_{Ti} and both R/L_{Te} and R/L_{ne} reduced by 20%. No rotation is included. The growth rate spectrum is shown in the left panel, and the frequency spectrum in the right panel.

below.

Firstly, the linear EM impact in Miller geometry for this parameter set is much reduced compared to the analogous $\hat{s} - \alpha$ case. This is seen in figure 15, showing a comparison between EM and ES linear calculations for nominal R/L_{Ti} and both R/L_{Te} and R/L_{ne} reduced by 20%. The linear impact of finite-β can be compared to the $\hat{s} - \alpha$ case in figure 10. α_{MHD} is kept fixed at the nominal value for both the EM and ES simulations. While in the $\hat{s} - \alpha$ case the growth rate reduction due to EM-effects was significant across the entire spectrum, in the Miller case the impact is much weakened, particularly at the transport driving scales at lower k_y. A weak linear EM-stabilization effect at outer radii was also observed in Ref. [28] with shaped geometry. The comparison between EM-stabilization in shaped and $\hat{s} - \alpha$ geometry was not carried out in previous work. An investigation regarding the physical provenance of the observed differences of EM-stabilization due to geometry is interesting also due to a possibility for performance optimization with shaping actuators, but is out of the scope of this paper.

Nevertheless, even though the linear impact is minor, significant EM-stabilization is still observed in the nonlinear GENE simulations with Miller geometry. This is seen in figure 16, showing the R/L_{Ti} scan at 20% reduced R/L_{Te} and R/L_{ne}, for both the (nominal) EM simulations as well as an ES scan. For both ES and EM cases, the transport is stiff with power balance reached in the proximity of the nonlinear R/L_{Ti} threshold. However, an R/L_{Ti} nonlinear threshold upshift on the order of $\approx 20\%$ is apparent in the EM scan compared to the ES scan. This is suggestive of finite-β effects extending the Dimits

shift regime [56], as in Ref. [57]. The upshift is of the same order of the ad-hoc threshold upshift EM-stabilization rule applied in QuaLiKiz, supporting its use. However, while encouraging, no general statement can yet be made regarding the validity of the QuaLiKiz ad-hoc EM-stabilization rule, as in other studies the primary impact of EM-stabilization was predicted to be a reduction of transport stiffness (slope of Q_i with respect to R/L_{Ti}) [28]. Additional work is necessary to untangle the parameterization and impact of EM-stabilization in reduced models.
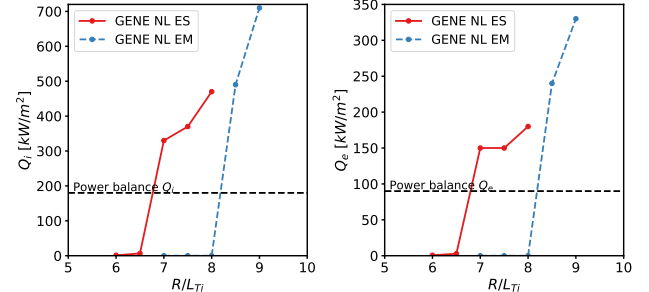

Figure 16: R/L_{Ti} scan from both electrostatic (red) vs electromagnetic (blue) nonlinear GENE simulations with Miller geometry. Both R/L_{Te} and R/L_{ne} are reduced by 20% from the nominal measured values (see table 3). The power balance heat fluxes from the integrated modelling run is portrayed by the horizontal dashed lines.

The heightened impact of zonal flows on the nonlinear threshold upshift in the electromagnetic simulation is evident in figure 17. Q_i time-traces are shown from the $R/L_{Ti} = 8$ EM and ES simulations at 20% reduced R/L_{Te} and R/L_{ne}. The electrostatic case is robustly unstable. The electromagnetic case, following the initial linear phase, transitions into a quiescent state dominated by zonal flows, as seen by the electrostatic potential contour map inset, where the flux asymptotically approaches zero.

Interestingly, while in previous work on gyrokinetic analysis of JET hybrid scenarios, a weak linear EM-stabilization at outer radii was also observed with

shaped geometry [28], the previous work also showed no significant nonlinear EM-stabilization in contrast to the present study. The most significant difference in parameters between the previous and present work, are the thermal R/L_{Ti} and R/L_{Te} values, which are much higher in the present study, likely owing to the increased heating power. These parameters contribute to the EM-mode drive, perhaps contributing to the stabilization. A detailed study is out of the scope of this work.
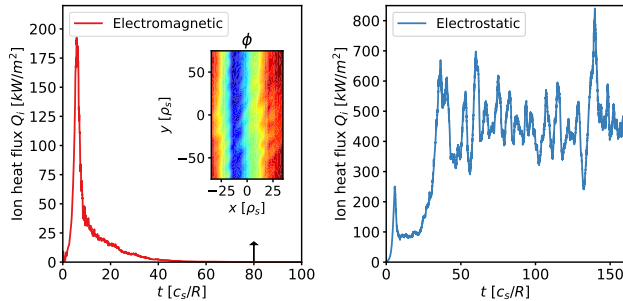

Figure 17: Comparison of electrostatic (right panel) and electromagnetic (left panel) nonlinear GENE simulation ion heat flux time series. $R/L_{Ti}= 8$ and both R/L_{Te} and R/L_{ne} are reduced by 20% from their nominal measured values. The EM case electrostatic potential contour at $t = 80$, at the z position corresponding to the LFS, is inset in the left panel.

An additional impact of EM-effects was observed on the ion-scale electron heat flux. With finite-β, the electron heat flux was observed to increase relative to the ion heat flux. The increase was in the electrostatic heat flux, with the electromagnetic heat flux (magnetic flutter) remaining negligible. The electron heat flux increase is likely dominated by linear effects, since a similar relative increase is seen both in linear and nonlinear simulations, as shown in figure 18. Averaging over the ion-scale k_y spectrum, the linear Q_i/Q_e decreased from 3.26 to 2.50 when transitioning from ES to EM simulations. The nonlinear case decreased from 2.86 to 2.01. We conjecture that this effect is related to the mechanism previously predicted to increase electron particle flux in finite-β gyrokinetic calculations [58]. The next section further explores this conjecture, which contributes towards reaching the experimental power balance of $Q_i/Q_e \approx 2$.

5 Analytic study of β-enhanced electron heat flux

This section derives an analytical model that isolates the impact of finite-β on the non-magnetic-flutter component of the electron heat flux. The derivation is strongly based on related work in Ref. [58] on the impact of finite-β on particle flux. The analytical model provides a prediction that the ion to electron heat flux ratio is decreased in the ITG
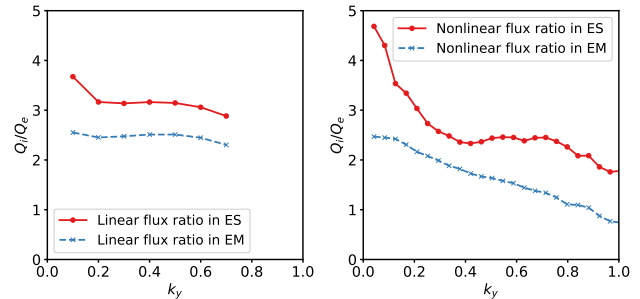

Figure 18: Comparison of ion to electron heat flux ratios in electrostatic and electromagnetic cases from linear GENE calculations (left panel) and Fourier decomposition of a nonlinear GENE simulation (right panel). $R/L_{Ti}= 8.5$, with both R/L_{Te} and R/L_{ne} reduced by 20% from their nominal measured quantities.

regime, and potentially increased in the TEM regime. This prediction is validated by dedicated numerical gyrokinetic calculations.

We now proceed with the derivation. The electron heat flux can be divided in trapped and passing components:

$$q_e = f_t q_{e,trap} + (1 - f_t)q_{e,pass} \tag{4}$$

where $q_{e,trap}$ and $q_{e,pass}$ are the respective trapped and passing electron contributions normalized to their population density. Finite-β effects only impact $q_{e,pass}$ due to the role of parallel velocity in Ampère's Law. As such, we concentrate on $q_{e,pass}$.

Closely following the derivation in Ref. [58], the general expression for the quasilinear electron heat flux, neglecting magnetic flutter terms, is:

$$q_{e,pass} \tag{5}$$
$$= \sum_k \left\langle k_y \rho_s c_s \int d^3 v E F_0 J \left[1 - 2v_\| \Omega_{r,k} + v_\|^2 \left(\Omega_{r,k}^2 + \Omega_{i,k}^2\right)\right] H \right\rangle$$

$$H = \tag{6}$$
$$\Phi^2 \frac{(\gamma_k + \nu)k_y \rho_s[\frac{R}{L_{ne}} + (E - \frac{3}{2}\frac{R}{L_{Te}})] - [\gamma_k(k_\| v_\| + \omega_{d,k}) - \omega_{r,k}\nu]}{(\omega_{r,k} + k_\| v_\| + \omega_{d,k})^2 + (\gamma_k + \nu)^2}$$

where E is normalized (to T_e) particle energy, J the Bessel function due to FLR effects, k the respective mode number, ν the collisionality, γ the mode growth rate, ω_r its real frequency, ω_d the ∇B drift frequency, and $\Omega_{r,k}, \Omega_{i,k}$ are the real and imaginary part of the quantity Ω defined as:

$$A_\| = \Omega \Phi \tag{7}$$

where $A_\|$ is the fluctuating vector potential, and Φ the fluctuating electrostatic potential. The terms proportional to Ω represent the contribution of β to the non-magnetic-flutter component of the electron heat flux. Upon solving the Ampère-Maxwell system, one finds that Ω, in the limit of large parallel velocity of

passing electrons, becomes:

$$\Omega_k \approx \frac{q\beta(k_y\rho_s R/L_{ne} + \omega_{r,k} + i\gamma)}{(k_\perp\rho_s)^2} \qquad (8)$$

In the low β limit, we neglect the terms proportional to Ω^2. Moreover, we take the limit $v_\parallel \to \infty$ (because of the mass ratio appearing when normalizing to c_s). The leading order term of the β-dependent $E\times B$ electron heat flux is then:

$$q_{e,pass,\beta} \qquad (9)$$
$$\approx \sum_k \left\langle k_y\rho_s c_s \int d^3v E F_0 J \left[-2v_\parallel\Omega_{r,k}\right] \Phi^2 \frac{-[\gamma_k k_\parallel v_\parallel]}{(k_\parallel v_\parallel)^2}\right\rangle$$

that is:

$$q_{e,pass,\beta} \qquad (10)$$
$$\approx \beta \sum_k \left\langle 2qk_y\rho_s c_s \frac{k_y\rho_s R/L_{ne} + \omega_{r,k}}{(k_\perp\rho_s)^2} \Phi^2 \frac{\gamma_k}{k_\parallel} \int d^3v E F_0 J\right\rangle$$

For ITG (positive ω), this gives an outward heat flux contribution, proportional to the plasma energy and β. For TEM (negative ω), particularly at non-extreme density peaking scenarios, this can lead to an inward heat flux contribution.

The analytic prediction of the differing sign of β-induced $E \times B$ electron heat flux for ITG modes vs TEMs is borne out by linear gyrokinetic simulations for the case studied here. Figure 19 shows the heat flux ratio for a linear spectrum, corresponding to the nominal measured inputs from table 3, with the modification of $R/L_{Ti}= 3$, such that TEMs are the dominant unstable modes. For the majority of the spectrum, the ES-case Q_i/Q_e flux ratio is now below the EM-case Q_i/Q_e flux ratio, as opposed to the ITG cases previously shown.
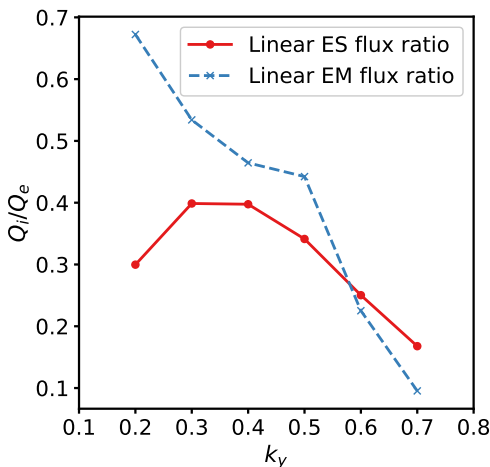

Figure 19: Comparison of ion to electron heat flux ratios in electrostatic and electromagnetic cases from linear GENE calculations corresponding to a TEM case. Nominal measured parameters are used apart from $R/L_{Ti}= 3$, such that TEMs dominate the spectrum.

6   Conclusions

The primary aim of this work was to validate predictions that in high T_i/T_e hybrid H-mode scenarios on JET, ETG turbulence plays an important role in clamping T_e, leading to increased T_i/T_e and improved ion thermal confinement at heavier isotopes (anti-Gyrobohm isotope confinement scaling), enabled due to a reduction in ion-electron heat exchange at heavier isotope. These previous results were obtained in integrated modelling with a version of QuaLiKiz in which the collision operator was incorrectly overly stabilizing TEMs [30]. Following improvements of the QuaLiKiz collision operator [45], these JET hybrid H-mode predictions were revisited both with the improved QuaLiKiz as well as high-fidelity nonlinear gyrokinetic single-scale and multiscale modelling. Understanding the role of ETG turbulence in these high-performance scenarios, and its impact on isotope confinement scaling, is of great importance towards physics interpretation of T and DT JET hybrid H-mode scenarios, and in validating reduced transport models applied for extrapolations towards ITER and reactors.

While the outlined mechanism is valid, the results in this paper invalidate the specific previous prediction by showing reduced evidence of the importance of ETG turbulence in this regime. Point-by-point conclusions are as follows. As a caveat, we stress that all gradient-driven analysis involving higher-fidelity GENE and GKV modelling are restricted to $\rho = 0.65$ of the analyzed JET discharge.

- Integrated modelling of a similar JET hybrid H-mode scenario as in Ref. [30] with QuaLiKiz-2.8.2 (improved collision operator) predicts a reduced significance of ETG turbulence and its corresponding anti-GyroBohm scaling effect. Unstable ETG is limited to the $\rho < 0.4$ region with QuaLiKiz-2.8.2, instead of broadly as predicted by the integrated modelling with QuaLiKiz-2.6.1.

- GENE modelling validates QuaLiKiz-2.8.2 ion-scale predictions in the power balance relevant regime, and invalidates QuaLiKiz-2.6.1 predictions which had too high Q_i/Q_e on ion scales due to over-suppression of TEM.

- GENE and GKV multiscale nonlinear simulations in an expected ETG-relevant regime with $(\gamma/k_y)_{\mathrm{maxETG}} > (\gamma/k_y)_{\mathrm{maxITG}}$, did not predict significant ETG flux. This suggests that additional hidden variables impact the emergence of multiscale ETG flux. Simple rules-of-thumb based on linear drive ratios may indicate the emergence of finite ETG flux above nonlinear thresholds, but not its significance, which depends on additional

quantities impacting streamer formation and multiscale interactions.

- GENE nonlinear ion-scale modelling with realistic geometry, rotation and EM effects at $\rho = 0.65$ was sufficient to recover the experimental power balance heat flux ratio without the need to invoke ETG turbulence. The power balance fluxes themselves were reproduced with R/L_{Ti} within 5%, and both R/L_{Te} and R/L_{ne} values within $\approx 20\%$, of the measured values.

The GENE nonlinear ion-scale analysis triggered further investigations regarding the impact of EM-effects on turbulence. These secondary conclusions are as follows:

- A significant difference in linear EM-stabilization of ITG modes was found between simulations with $\hat{s} - \alpha$ and more realistic shaped Miller geometry. The linear EM-stabilization impact was reduced with Miller geometry. However, with Miller geometry a significantly enhanced Dimits shift regime was observed in nonlinear simulations, leading to a 20% increase in R/L_{Ti}, key to reaching power balance fluxes within experimental gradient error bars. The nature and magnitude of the threshold upshift supports the ad-hoc EM-stabilization model in QuaLiKiz.

- An increase in the $E \times B$ component of the electron heat flux relative to the ion heat flux was observed in the finite-β GENE linear and nonlinear simulations. This increase contributes to predicting the inferred heat flux ratio. The effect is related to previous predictions in Ref. [58] of the β impact on electron particle transport. An analytical prediction of opposite (increased Q_i/Q_e with finite-β) behaviour for TEM-driven heat flux was validated by gyrokinetic calculations.

In general, this work has further illustrated the difficulties of carrying out a multiscale validation effort with realistic parameters. EM effects, impurities, magnetic geometry, and rotation all play key roles in setting the turbulence level. EM effects and impurities increase the required computation time such that extensive validation efforts with uncertainty quantification and numerical convergence checking is barely feasible with current resources. Nevertheless, these inputs are necessary for physical consistency and future efforts should push the envelope in this direction. The inclusion of rotation complicates linking the turbulence predictions with inputs corresponding to power-balance fluxes, to the underlying linear instability drive (e.g. the relative ITG and ETG γ/k ratios) due to the time-dependence induced on the linear modes. This further complicates the utility of linear-based metrics for estimating the onset of multiscale effects.

Finally, we stress that while the specific prediction in Ref. [30] was not validated by this work, the basic mechanism of ETG-induced anti-GyroBohm scaling is valid. We cannot rule out the emergence of this effect in discharges with further increased T_i/T_e, such as the high performance scenarios recently developed at JET [59].

7 Acknowledgements

References

[1] F. M. Poli, "Integrated Tokamak modeling: When physics informs engineering and research planning," *Physics of Plasmas*, vol. 25, no. 5, p. 055 602, 2018.

[2] X Garbet, Y Idomura, L Villard, and T. Watanabe, "Gyrokinetic simulations of turbulent transport," *Nucl. Fusion*, vol. 50, no. 4, p. 043 002, 2010.

[3] A. White, "Validation of nonlinear gyrokinetic transport models using turbulence measurements," *Journal of Plasma Physics*, vol. 85, no. 1, 2019.

[4] C Bourdelle, J Citrin, B Baiocchi, A Casati, P Cottier, X Garbet, F Imbeaux, and J. Contributors, "Core turbulent transport in tokamak plasmas: bridging theory and experiment with QuaLiKiz," *Plasma Physics and Controlled Fusion*, vol. 58, no. 1, p. 014 036, 2015.

[5] J. Citrin, C. Bourdelle, F. Casson, C. Angioni, N. Bonanomi, Y. Camenen, X. Garbet, L. Garzotti, T. Görler, O. Gürcan, F. Koechl, F. Imbeaux, O. Linder, K. van de Plassche, P. Strand, and G. S. J. contributors, "Tractable flux-driven temperature, density, and rotation profile evolution with the quasilinear gyrokinetic

transport model QuaLiKiz," *Plasma Physics and Controlled Fusion*, vol. 59, no. 12, p. 124 005, 2017.

[6] G. Staebler, J. Kinsey, and R. Waltz, "A theory-based transport model with comprehensive physics," *Phys. Plasmas*, vol. 14, p. 055 909, 2007.

[7] W. Dorland, F. Jenko, M. Kotschenreuther, and B. Rogers, "Electron temperature gradient turbulence," *Phys. Rev. Lett.*, vol. 85, p. 5579, 2000.

[8] F. Jenko and W. Dorland, "Prediction of significant tokamak turbulence at electron gyroradius scales," *Phys. Rev. Lett.*, vol. 89, pp. 225 001–1, 2002.

[9] S. P. Smith, C. C. Petty, A. E. White, C. Holland, R. Bravenec, M. E. Austin, L. Zeng, and O. Meneghini, "Electron temperature critical gradient and transport stiffness in DIII-D," *Nuclear Fusion*, vol. 55, no. 8, p. 083 011, 2015.

[10] F Ryter, C Angioni, M Dunne, R Fischer, B Kurzan, A Lebschy, R. McDermott, W Suttrop, G Tardini, E Viezzer, *et al.*, "Heat transport driven by the ion temperature gradient and electron temperature gradient instabilities in ASDEX Upgrade H-modes," *Nuclear Fusion*, vol. 59, no. 9, p. 096 052, 2019.

[11] N Bonanomi, P Mantica, J Citrin, T Goerler, B Teaca, and J. Contributors, "Impact of electron-scale turbulence and multi-scale interactions in the JET tokamak," *Nuclear Fusion*, vol. 58, no. 12, p. 124 003, 2018.

[12] A Mariani, P Mantica, S Brunner, M Fontana, A Karpushov, C Marini, L Porte, O Sauter, T. Team, E. M. Team, *et al.*, "Investigation of the role of electron temperature gradient modes in electron heat transport in TCV plasmas," *Nuclear Fusion*, vol. 59, no. 12, p. 126 017, 2019.

[13] P Mantica, N Bonanomi, A Mariani, P Carvalho, E Delabie, J Garcia, N Hawkes, T Johnson, D Keeling, M Sertoli, *et al.*, "The role of electron-scale turbulence in the JET tokamak: experiments and modelling," *Nuclear Fusion*, vol. 61, no. 9, p. 096 014, 2021.

[14] G. Colyer, A. Schekochihin, F. Parra, C. Roach, M. Barnes, Y. Ghim, and W Dorland, "Collisionality scaling of the electron heat flux in ETG turbulence," *Plasma Physics and Controlled Fusion*, vol. 59, no. 5, p. 055 002, 2017.

[15] S Maeyama, Y Idomura, T.-H. Watanabe, M Nakata, M Yagi, N Miyato, A Ishizawa, and M Nunami, "Cross-scale interactions between electron and ion scale turbulence in a tokamak plasma," *Physical review letters*, vol. 114, no. 25, p. 255 002, 2015.

[16] N. T. Howard, A. E. White, M. Greenwald, C. Holland, and J. Candy, "Multi-scale gyrokinetic simulation of Alcator C-Mod tokamak discharges," *Phys. Plasmas*, vol. 21, p. 032 308, 201. DOI: `http://dx.doi.org/10.1063/1.4869078`.

[17] N. Howard, C. Holland, A. White, M. Greenwald, and J. Candy, "Multi-scale gyrokinetic simulation of tokamak plasmas: Enhanced heat loss due to cross-scale coupling of plasma turbulence," *Nucl. Fusion*, vol. 56, no. 1, p. 014 004, 2016.

[18] C Holland, N. Howard, and B. Grierson, "Gyrokinetic predictions of multiscale transport in a DIII-D ITER baseline discharge," *Nuclear Fusion*, vol. 57, no. 6, p. 066 043, 2017.

[19] N. T. Howard, C. Holland, A. E. White, M. Greenwald, J. Candy, and A. J. Creely, "Multi-scale gyrokinetic simulations: Comparison with experiment and implications for predicting turbulence and transport," *Phys. Plasmas*, vol. 23, p. 056 109, 2016. DOI: `http://dx.doi.org/10.1063/1.4946028`.

[20] G. Staebler, N. Howard, J. Candy, and C. Holland, "A model for the coupling of electron and ion scale gyrokinetic turbulence," *Nucl. Fusion*, vol. 57, p. 066 046, 2017. DOI: `https::/doi.org/10.1088/1741-4326/aa6bee`.

[21] A. J. Creely, P Rodriguez-Fernandez, G. D. Conway, S. J. Freethy, N. T. Howard, A. E. White, and the ASDEX Upgrade Team, "Criteria for the importance of multi-scale interactions in turbulent transport simulations," *Plasma Physics and Controlled Fusion*, vol. 61, p. 085 022, 2019.

[22] G. Staebler, J. Candy, N. T. Howard, and C. Holland, "The role of zonal flows in the saturation of multi-scale gyrokinetic turbulence," *Phys. Plasmas*, vol. 23, p. 062 518, 2016. DOI: `https://doi.org/10.1063/1.4954905`.

[23] B. A. Grierson, G. M. Staebler, W. M. Solomon, G. R. McKee, C. Holland, M. Austin, A. Marinoni, L. Schmitz, and R. I. Pinsker, "Multi-scale transport in the DIII-D ITER baseline scenario with direct electron heating and projection to ITER," *Physics of Plasmas*, vol. 25, no. 2, p. 022 509, 2018. DOI: `10.1063/1.5011387`.

[24] E Joffrin, A. Sips, J. Artaud, A Becoulet, L Bertalot, R Budny, P Buratti, P Belo, C. Challis, F Crisanti, *et al.*, "The 'hybrid' scenario in JET: Towards its validation for ITER," *Nuclear fusion*, vol. 45, no. 7, p. 626, 2005.

[25] J Hobirk, F Imbeaux, F Crisanti, P Buratti, C. Challis, E Joffrin, B Alper, Y Andrew, P Beaumont, M Beurskens, *et al.*, "Improved confinement in JET hybrid discharges," *Plasma Physics and Controlled Fusion*, vol. 54, no. 9, p. 095 001, 2012.

[26] C. D. Challis, J Garcia, M Beurskens, P Buratti, E Delabie, P Drewelow, L. Frassinetti, C Giroud, N Hawkes, J Hobirk, *et al.*, "Improved confinement in JET high beta plasmas with an ITER-like wall," *Nuclear Fusion*, vol. 55, no. 5, p. 053 031, 2015.

[27] J Garcia, C Challis, J Citrin, H Doerk, G Giruzzi, T Görler, F Jenko, P Maget, and J. Contributors, "Key impact of finite-beta and fast ions in core and edge tokamak regions for the transition to advanced scenarios," *Nuclear Fusion*, vol. 55, no. 5, p. 053 007, 2015.

[28] J Citrin, J Garcia, T Görler, F Jenko, P Mantica, D Told, C Bourdelle, D. Hatch, G. Hogeweij, T. Johnson, *et al.*, "Electromagnetic stabilization of tokamak microturbulence in a high-beta regime," *Plasma Physics and Controlled Fusion*, vol. 57, no. 1, p. 014 032, 2014.

[29] F. Jenko, W. Dorland, and G. Hammett, "Critical gradient formula for toroidal electron temperature gradient modes," *Phys. Plasmas*, vol. 8, p. 4096, 2001.

[30] F. J. Casson, H. Patten, C. Bourdelle, S. Breton, J. Citrin, F. Koechl, M. Sertoli, C. Angioni, Y. Baranov, R. Bilato, *et al.*, "Predictive multi-channel flux-driven modelling to optimise ICRH tungsten control and fusion performance in JET," *Nuclear Fusion*, 2020.

[31] G. Cenacchi and A. Taroni, "JETTO: A free boundary plasma transport code," ENEA, Rome (Italy), Tech. Rep., 1988.

[32] M Romanelli, G Corrigan, V Parail, S Wiesen, R Ambrosino, P. d. S. A. Belo, L Garzotti, D Harting, F Köchl, T Koskela, *et al.*, "JINTRAC: A system of codes for integrated simulation of tokamak scenarios," *Plasma Fusion Res*, 2014.

[33] E. Belli, J Candy, and R. Waltz, "Reversal of simple hydrogenic isotope scaling laws in tokamak edge turbulence," *Physical Review Letters*, vol. 125, no. 1, p. 015 001, 2020.

[34] A. Mariani, P. Mantica, I. Casiraghi, J. Citrin, T. Görler, G. M. Staebler, and J. EUROfusion, "Benchmark of quasi-linear models against gyrokinetic single scale simulations in deuterium and tritium plasmas for a JET high beta hybrid discharge," *Nuclear Fusion*, vol. 61, no. 6, p. 066 032, 2021.

[35] M Sertoli, P. J. Carvalho, C Giroud, S Menmuir, and J. Contributors, "Measuring the plasma composition in tokamaks with metallic plasma-facing components," *Journal of Plasma Physics*, vol. 85, no. 5, 2019.

[36] L. Lao, H. S. John, R. Stambaugh, A. Kellman, and W. Pfeiffer, "Reconstruction of current pro-file parameters and plasma shapes in tokamaks," *Nucl. Fusion*, vol. 25, p. 1611, 1985.

[37] L. Appel, I Lupelli, and J. Contributors, "Equilibrium reconstruction in an iron core tokamak using a deterministic magnetisation model," *Computer Physics Communications*, vol. 223, pp. 1–17, 2018.

[38] Szepesi, G., et al. "Advanced equilibrium reconstruction for JET with EFIT++", 47th EPS Conference on Plasma Physics, 2020.

[39] A Ho, J Citrin, F Auriemma, C Bourdelle, F. Casson, H.-T. Kim, P Manas, G Szepesi, H Weisen, and J. Contributors, "Application of gaussian process regression to plasma turbulent transport model validation via integrated mod-elling," *Nuclear Fusion*, vol. 59, no. 5, p. 056 007, 2019.

[40] J. Breslau *et al.*, *Transp website: Https://transp.pppl.gov.* DOI: `https : / / doi . org / 10 . 11578 / dc . 20180627.4`.

[41] R. J. Goldston, D. McCune, H. Towner, S. Davis, R. Hawryluk, and G. Schmidt, "New techniques for calculating heat and particle source rates due to neutral beam injection in axisymmetric tokamaks," *Journal of computational physics*, vol. 43, no. 1, pp. 61–78, 1981.

[42] M. Brambilla, "Quasi-local wave equations in toroidal geometry with applications to fast wave propagation and absorption at high harmonics of the ion cyclotron frequency," *Plasma physics and controlled fusion*, vol. 44, no. 11, p. 2423, 2002.

[43] C. D. Stephens, X. Garbet, J. Citrin, C. Bourdelle, K. L. van de Plassche, and F. Jenko, "Quasilinear gyrokinetic theory: a derivation of QuaLiKiz," *Journal of Plasma Physics*, vol. 87, no. 4, 2021.

[44] F. Jenko, W. Dorland, M. Kotschenreuther, and B. Rogers, "Electron temperature gradient driven turbulence," *Phys. Plasmas*, vol. 7, p. 1904, 2000.

[45] C. Stephens *et al.*, to be submitted to Phys. Plasmas (2021).

[46] W. A. Houlberg, K. C. Shaing, S. P. Hirshman, and M. C. Zarnstorff, "Bootstrap current and neoclassical transport in tokamaks of arbitrary collisionality and aspect ratio," *Physics of Plasmas*, vol. 4, no. 9, pp. 3230–3242, 1997. DOI: 10.1063/1.872465.

[47] N. Kumar, Y. Camenen, S. Benkadda, C. Bourdelle, A. Loarte, A. R. Polevoi, F. Widmer, *et al.*, "Turbulent transport driven by kinetic ballooning modes in the inner core of JET hybrid H-modes," *Nuclear Fusion*, vol. 61, no. 3, p. 036 005, 2021.

[48] P Cottier, C Bourdelle, Y Camenen, Ö. D. Gürcan, F. Casson, X. Garbet, P Hennequin, and T. Tala, "Angular momentum transport modeling: Achievements of a gyrokinetic quasi-linear approach," *Plasma Physics and Controlled Fusion*, vol. 56, no. 1, p. 015 011, 2013.

[49] R. Miller, M. Chu, J. Greene, Y. Lin-liu, and R. Waltz, "Non-circular, finite aspect ratio, local equilibrium model," *pop*, vol. 5, p. 973, 1998.

[50] A Di Siena, T Görler, E Poli, A. B. Navarro, A Biancalani, R Bilato, N Bonanomi, I Novikau, F Vannini, and F Jenko, "Nonlinear electromagnetic interplay between fast ions and ion-temperature-gradient plasma turbulence," *Journal of Plasma Physics*, vol. 87, no. 2, 2021.

[51] H Doerk, M Dunne, F Jenko, F Ryter, P. Schneider, E Wolfrum, and A. U. Team, "Electromagnetic effects on turbulent transport in high-performance ASDEX Upgrade discharges," *Physics of Plasmas*, vol. 22, no. 4, p. 042 503, 2015.

[52] T.-H. Watanabe and H Sugama, "Velocity–space structures of distribution function in toroidal ion temperature gradient turbulence," *Nuclear Fusion*, vol. 46, no. 1, p. 24, 2005.

[53] S. Maeyama, A. Ishizawa, T.-H. Watanabe, N. Nakajima, S. Tsuji-Iio, and H. Tsutsui, "Numerical techniques for parallel dynamics in electromagnetic gyrokinetic Vlasov simulations," *Computer Physics Communications*, vol. 184, no. 11, pp. 2462–2473, 2013.

[54] S Maeyama, T.-H. Watanabe, and A Ishizawa, "Suppression of ion-scale microtearing modes by electron-scale turbulence via cross-scale nonlinear interactions in tokamak plasmas," *Physical Review Letters*, vol. 119, no. 19, p. 195 002, 2017.

[55] G. M. Staebler, J. Candy, E. A. Belli, J. E. Kinsey, N Bonanomi, and B. Patel, "Geometry dependence of the fluctuation intensity in gyrokinetic turbulence," *Plasma Physics and Controlled Fusion*, vol. 63, no. 1, p. 015 013, 2021.

[56] A. Dimits, G. Bateman, M. Beer, B. Cohen, W. Dorland, G. Hammett, C. Kim, J. Kinsey, M. Kotschenreuther, A. Kritz, L. Lao, J. Mandrekas, W. Nevins, S. Parker, A. Redd, D. Shumaker, R. Sydora, and J. Weiland, "Comparisons and physics basis of tokamak transport models and turbulence simulations," *Phys. Plasmas*, vol. 7, p. 969, 2000.

[57] M. Pueschel and F Jenko, "Transport properties of finite-β microturbulence," *Physics of Plasmas*, vol. 17, no. 6, p. 062 307, 2010.

[58] T Hein, C Angioni, E Fable, and J Candy, "Gyrokinetic study of the role of β on electron particle transport in tokamaks," *Physics of Plasmas*, vol. 17, no. 10, p. 102 309, 2010.

[59] J Garcia, E de la Luna, M Sertoli, F Casson, S Mazzi, Z Stancar, G Szepesi, D Frigione, L Garzotti, F Rimini, *et al.*, "New plasma regimes with small ELMs and high confinement at the Joint European Torus," *arXiv preprint arXiv:2103.02679*, 2021.